

Electronic Supplementary Information (ESI).

Coupling molecular spin centers to microwave planar resonators: towards integration of molecular qubits in quantum circuits

C. Bonizzoni, A. Ghirri, K. Bader, J. van Slageren, M. Perfetti, L. Sorace, Y. Lan, O. Fuhr, M. Ruben
and M. Affronte

YBCO coplanar resonator

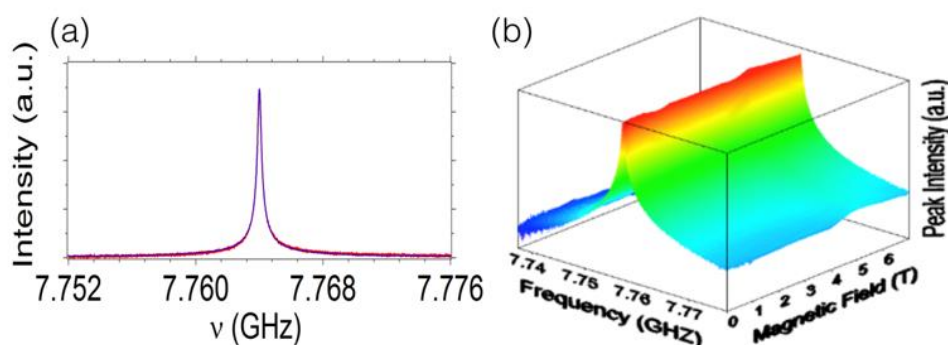


Figure S1: (a) Zero-field transmission spectrum of the bare resonator measured at 2 K ($P_{in} = -13$ dBm). Blue line is a fitting based on eq. (2).
(b) 3D plot showing the evolution of the resonant peak as a function of the external magnetic field ($T=2$ K).

The resonator is fabricated on a YBCO (330 nm)/sapphire ($430 \mu\text{m}$) film ($T_c = 87$ K) by means of optical lithography and wet chemical etching [1]. The top view of the resonator geometry is shown in Figure 1 of the main text. The central strip has a width $w = 200 \mu\text{m}$ and a length $L = 8$ mm, while the separation from the lateral ground planes is $S = 73 \mu\text{m}$ (Figure 1 of the main paper). The resonance frequency of the half-wavelength fundamental mode is given by

$$\nu_0 = \frac{c}{2n_{eff}L} \quad (S1)$$

where c is speed of light in vacuum and n_{eff} is the effective refractive index of the device [2]. The transmission spectrum measured at 2 K is plotted in Figure S1(a). The line shape can be fitted by a Lorentzian function [3]

$$T(\nu) = \frac{T(\nu_0)}{1+Q_0^2\left(\frac{\nu-\nu_0}{\nu}\right)^2} \quad (S2)$$

where ν_0 is the resonant frequency, Q_0 is the quality factor, and $T(\nu_0)$ is the maximum of the transmission. The best fit is obtained with $\nu_0=7.7$ GHz and $Q_0=33000$ (Figure S1a). The resonator decay rate, which is defined as $k_0 = \nu_0/Q_0$, thus results $k_0 = 0.33$ MHz. We carried out transmission spectroscopy measurements in presence of an external magnetic field, which is applied parallel to the superconducting film, along the longest side of the central strip (Figure 1 of the main paper). The transmission spectral map is acquired by measuring frequency sweeps at each progressive step of the applied magnetic field. Figure S1(b) shows the transmission spectral map measured on the bare resonator at 2 K. The evolution of the transmission spectrum in the field range 0-7 T shows a weak dependence of both ν_0 and Q_0 from the applied magnetic field and it's discussed in detail in [1].

To perform transmission spectroscopy on molecular spin systems, we positioned a single crystal of molecular spins in the centre of the resonator (Figure 1 of the main paper). This position corresponds to the magnetic antinode of the fundamental electromagnetic mode of the cavity, where the coupling between spins and microwave field is maximized.

[ErPc₂]⁻TBA⁺ Additional Structural Information

The erbium ion occupies a central position in the complex and is eight-fold coordinated by the isoindole nitrogen atoms (N_{iso}) of the phthalocyanine ligands. The central erbium ion lies 1.381 Å from the N_{iso} mean plane of the Pc ligands. The distance between the nearest erbium ions is 14.776 Å. Both phthalocyanine ligands of [ErPc₂]⁻TBA⁺ complex are found to be distorted from planarity and adopt a biconcave shape. CCDC-1477855 ([ErPc₂]⁻TBA⁺) contains the supplementary crystallographic data for this paper. These data can be obtained free of charge at www.ccdc.cam.ac.uk/conts/retrieving.html (or from the Cambridge Crystallographic Data Centre, 12 Union Road, Cambridge CB2 1EZ, UK; fax: (internat.) +44-1223/336-033).

Additional Cu(mnt)₂ Results

Transmission spectroscopy results for the pure Cu(mnt)₂ crystal (2K, -43dBm) are shown in Fig. S2. Four clear frequency shift in the dispersion and their corresponding absorptions are visible in the *g*=2 region. This is consistent with what is expected from Copper (*S*=1/2, *l*=3/2). The angle dependence for the pure sample at 2K is shown in Fig. S3. Since we used non indexed single crystals, we don't have direct knowledge of the orientation of the molecules with respect to the static magnetic field. Basing on the structural information of [4], the crystal cell is monocline and the oblique *a*-axis can be easily recognized. As a consequence, we glue the crystals with the *bc* plane parallel to the plane of the resonator. From X-band CW EPR experiments at room temperature, the separation of the signals given by the two molecular orientations is $\delta B \approx 5mT$. Since the linewidth of Figure S2 are on the order of $\delta B \approx 100mT$, the signals from the two magnetic species cannot be resolved, giving only four lines. Nevertheless, to understand which one between the *b* and the *c* axis is parallel to the magnetic field for $\theta=0^\circ$, we compare our measurements with the easy spin simulation (Figure S3 (right)). The calculations were repeated for different angles between the molecular *z* axis and the static magnetic field and, for simplicity, only one of the two molecular orientation was computed. A qualitative estimation (red line of Figure S3 (right)) shows that agreement between measurements and calculation is found for an angle between *B*₀ and the molecular *z*-axis of 27°. According to the structural information, we deduce that $\theta=0^\circ$ corresponds to the situation in which the *c* axis parallel to the static magnetic field.

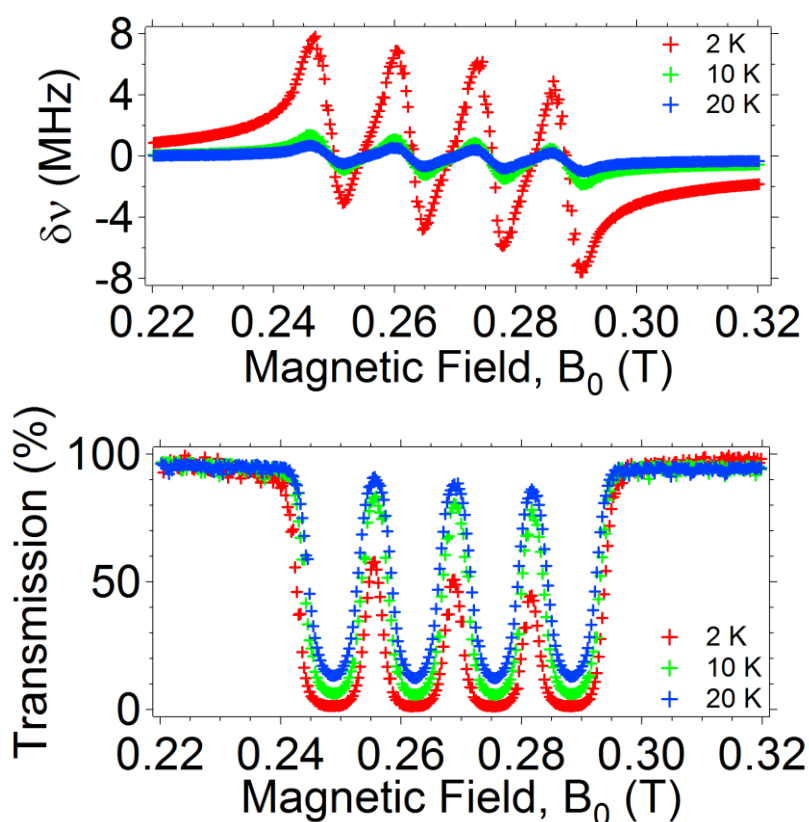


Figure S2: Frequency shift (top) and transmission (bottom) for the pure Cu(mnt)₂ (*P*_{in} = -43 dBm) at different temperatures.

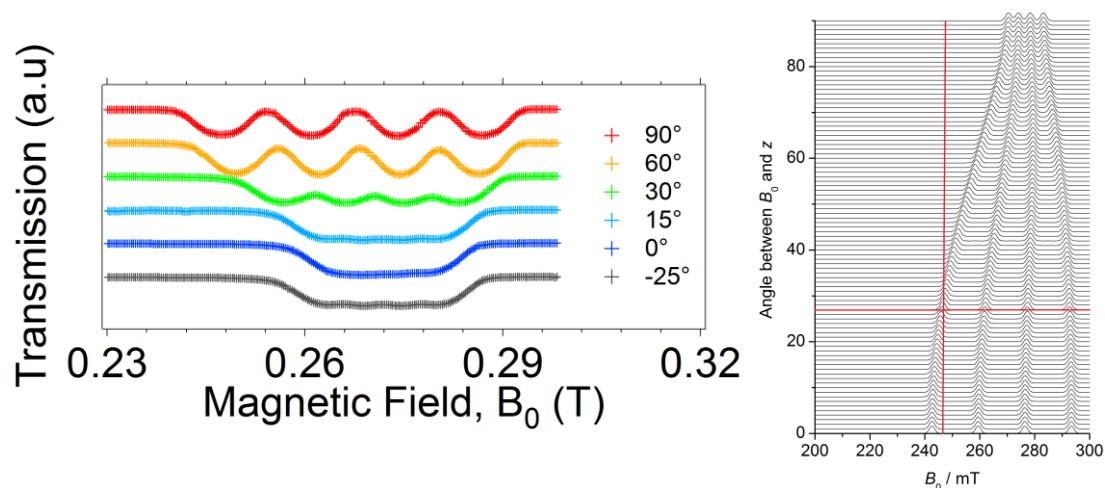


Figure S3: (left) Transmission for the pure Cu(mnt)_2 ($P_{in} = -43$ dBm) at 2K for different angles between the static magnetic field and the crystal c-axis. (right) Simulation of the transmission spectra performed with the Easyspin software. Calculation is done for different angles between the molecular z axis and the static magnetic field. Red lines correspond to the values which agrees with the transmission at $\theta=90^\circ$

Additional $\text{ErPc}_2\text{TBA}^+$ results

Results for the 10% $\text{ErPc}_2\text{TBA}^+$ crystals for $\theta=0,90^\circ$ at 2 K are shown in Fig. S4. The signal position changes, reflecting the magnetic anisotropy of the sample. Also the number of the structures and the widths drastically change with the orientation. Comparison between the pure and the 10% crystals at 2K ($\theta=90^\circ$) is reported in Fig. S5. Broadening effects of the line are visible for the pure sample and can be ascribed to the higher dipolar interaction between different ErPc_2 molecules. Additional fitting parameters based on Eqn (1) of the main paper are reported in Table S1.

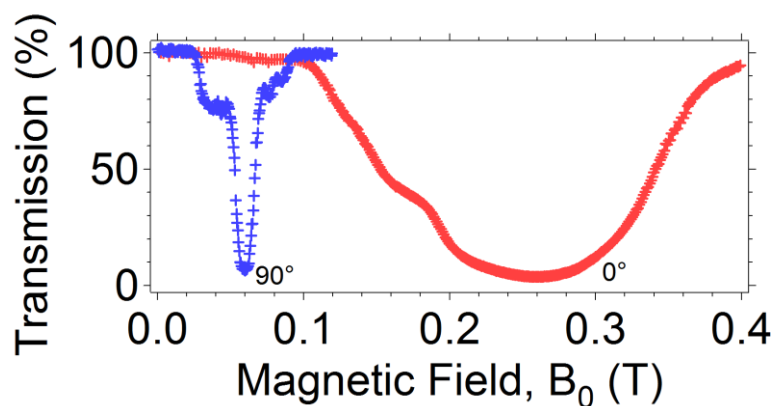


Figure S4: Transmission for the 10% ErPc_2 sample (2K, $P_{in} = -43$ dBm) for two different angles between the static magnetic field and the crystal c-axis.

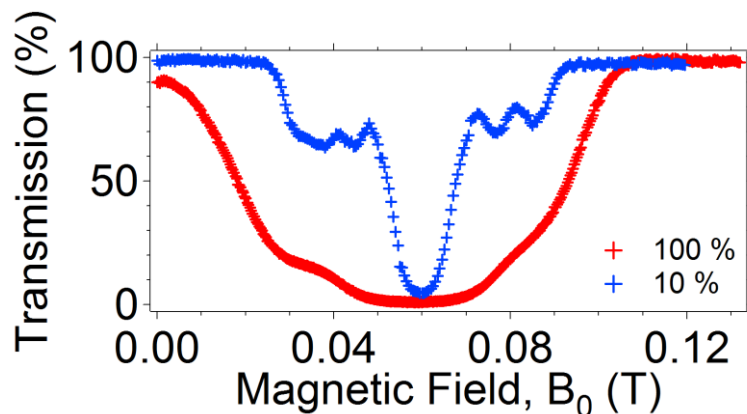


Figure S5: Transmission for the pure ErPc_2 sample (2K, $P_{in} = -43$ dBm) for two different angles between the static magnetic field and the crystal c-axis.

Sample	θ	g-factor	γ (MHz)	N_{eff} (T=2K)	g_c (MHz)	g_s (Hz)
10%	0	2.21 ± 0.22	897 ± 7	$7.6 \cdot 10^{14}$	60 ± 3	2.20 ± 0.22
10%	90	9.21 ± 0.01	410 ± 10	$6.5 \cdot 10^{14}$	27.1 ± 3.0	1.0 ± 0.2
100%	90	9.251 ± 0.02	1462 ± 50	$5.1 \cdot 10^{14}$	120 ± 4	5.30 ± 0.55
100%	0	2.30 ± 0.03	1232 ± 180	$6.0 \cdot 10^{14}$	130 ± 7	5.3 ± 1.0

Table S1: Additional fitting results for the ErPc₂ samples at 2K. The input powers is -43 dBm for the pure sample and -63 dBm for the 10% concentration.

Additional Dy(trensral) results

Results for the 0.6% Dy(trensral) for $\theta=0^\circ, 90^\circ$ at 2K are shown in Fig. S6. The position of the signal move to lower g-factors, the structure and the linewidths change. In particular, the measure taken at $\theta=0^\circ$ shows a main signal at $B_0 \approx 0.29\text{T}$ and additional signals at $B_0 \approx 0.15\text{T}$, $B_0 \approx 0.21\text{T}$, $B_0 \approx 0.23\text{T}$ and at $B_0 \approx 0.32\text{T}$. The peak at $B_0 \approx 0.29\text{T}$ corresponds to an effective $g_{\parallel} = 1.83$, which agrees well with the effective g_{\parallel} value obtained by standard EPR in ref. [5]. On the other hand, the presence of weak additional transitions can be attributed to the hyperfine contributions of the odd Dy isotopes. Comparison between the 3% and 0.6% crystals at 2 K for $\theta=90^\circ$ (Figure S7) shows that that is no more convenient to further increase the dilution, since the limit given by the inhomogeneous broadening of the sample is reached. Table S2 shows additional fitting parameters based on Eqn 1 of the main paper.

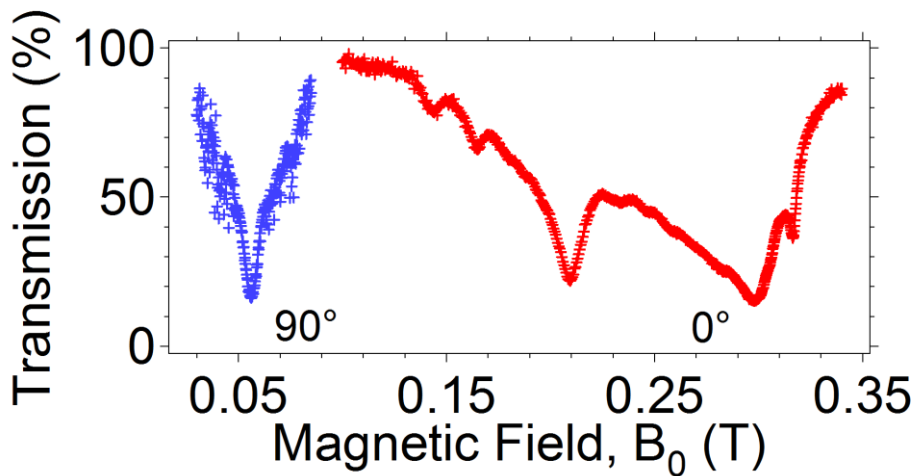


Figure S6: Transmission for the 0.6% Dy(trensral) ($P_{\text{in}} = -55$ dBm) at 2K for two different angles between the static magnetic field and the crystal c-axis. The additional peak at $\approx 0.18\text{T}$ is due to the contamination of the solvent during synthesis processes.

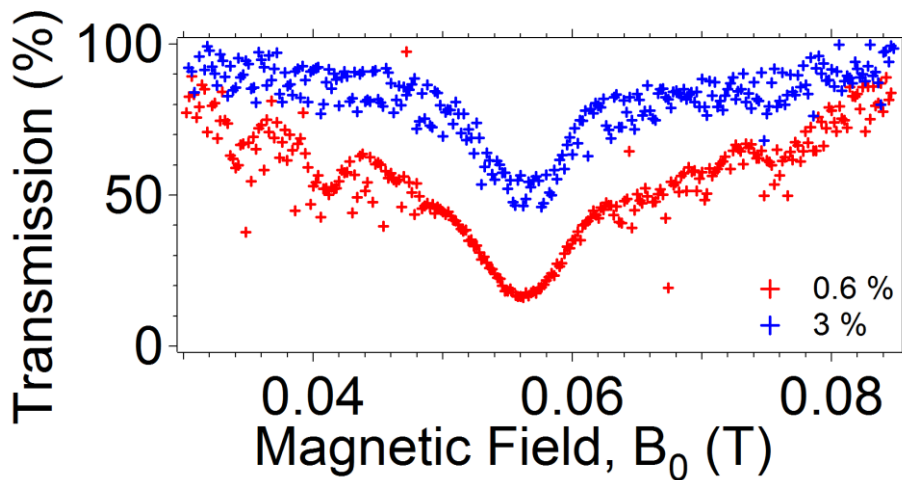


Figure S7: Comparison of the transmission of 0.6% and 0.3% Dy(trensral) (2K, $P_{\text{in}} = -55$ dBm) for $\theta=90^\circ$.

Sample	θ	Landè g-factor	γ (MHz)	N_{eff} (T=2K)	g_c (MHz)	g_s (Hz)
3%	90	9.93 ± 0.02	471 ± 38	$8 \cdot 10^{13}$	16.2 ± 2.0	1.82 ± 0.3
0.6%	90	9.87 ± 0.09	386 ± 88	$6.4 \cdot 10^{14}$	11.5 ± 6.6	0.53 ± 0.08

Table S2: Additional fitting results for the Dy(trensals) samples at 2K. The input powers is -55 dBm.

References

- [1] A. Ghirri, C. Bonizzoni, D. Gerace, S. Sanna, A. Cassinese and M. Affronte, *Appl. Phys. Lett.*, 2015, **106**, 184101.
- [2] R. N. Simons, *Coplanar Waveguide Circuits, Components and Systems* (Wiley-Interscience, 2001).
- [3] M. Hein, *High-Temperature Superconductors Thin Films at Microwave Frequency* (Springer, Berlin, 1999).
- [4] G. R. Lewis and I. Dance, *J. Chem. Soc., Dalton Trans.*, 2000, 3176.
- [5] E. Lucaccini, L. Sorace, M. Perfetti, J.-P. Costes and R. Sessoli, *Chem. Commun.*, 2014, **50**, 1648.